N. Tilton, L. Cortelezzi
Stability of Boundary Layers over Porous Walls with Suction
AIAA Journal, Vol. 53, N. 10, 2015, p. 2856-2868
doi:10.2514/1.J053716

Stability of Boundary Layers over Porous Walls With Suction

Nils Tilton[a]
Colorado School of Mines, Golden, Colorado, 80401, U.S.A.

Luca Cortelezzi[b]
McGill University, Montreal, Québec, H3A 0C3, Canada

Though there is considerable interest in using wall-suction to increase boundary layer stability, stability analyses suggest that porous walls are inherently destabilizing. We explore this contradiction by performing a spatial linear stability analysis of the asymptotic suction boundary layer using a realistic model of wall suction. The porous wall is modelled as a layer of rigid, homogeneous, isotropic, porous material of small permeability, in which inertial effects may be neglected. The porous layer is bounded above by a semi-infinite region in which a boundary layer is driven by a constant free-stream velocity. The wall suction is created by applying a suction pressure to a semi-infinite region below the porous layer. Our stability analysis takes account of the full coupling between the flow fields in the boundary layer and suction region, governed by the Navier-Stokes equations, and the flow in the porous layer, governed by the volume-averaged Navier-Stokes equations. We find that small amounts of wall permeability destabilize the Tollmien-Schlichting wave and cause a substantial broadening of the unstable region. As a result, the stabilization of boundary layers by wall-suction is substantially less effective and more expensive than what is predicted by classical boundary layer theory.

[a] Assistant Professor, Department of Mechanical Engineering, Brown Hall, 1610 Illinois Street, Golden, Colorado 80401; ntilton@mines.edu.

[b] Associate Professor, Department of Mechanical Engineering, 817 Sherbrooke St. West, Montreal, Québec, H3A 0C3; crtlz@cim.mcgill.ca

Nomenclature

Roman symbols

c = phase speed

d_1 = boundary layer displacement thickness when the permeability is zero

d_{99} = boundary layer thickness when the permeability is zero

D = indicates d/dy

$\mathcal{D}$ = discrete holes diameter

f = admittance

F = non-dimensional frequency $10^6\omega/Re$

F_c = critical non-dimensional frequency

$\mathbf{F}$ = Forchheimer's tensor

i = imaginary unit $\sqrt{-1}$

k = permeability

l_f = characteristic length associated with the fluid phase of the porous layer

l_{sl} = characteristic length associated with the solid phase of the porous layer

L_p = thickness of the porous layer

p = pressure

$\hat{p}$ = planar wave pressure perturbation

$\tilde{p}$ = amplitude of planar wave pressure perturbation

p_w = perturbation pressure at the wall

$\langle p \rangle^f$ = intrinsic volume-averaged pressure

P_s = suction pressure

P_∞ = free-stream pressure

r = radius of the averaging volume $\mathcal{V}$

Re = Reynolds number

Re_c = critical Reynolds number

t = time

$\widetilde{u}$ = amplitude of the streamwise velocity perturbation

U = non-dimensional streamwise laminar flow velocity

$\langle U \rangle$ = non-dimensional volume-averaged streamwise laminar flow velocity

U_∞ = free-stream velocity

$\mathbf{v} = [u\ v\ w]^T$ = velocity vector and its components

$\hat{\mathbf{v}} = [\hat{u}\ \hat{v}\ \hat{w}]^T$ = velocity vector of the planar wave perturbation and its components

$\widetilde{v}$ = amplitude of the wall-normal velocity perturbation

$\widetilde{v}_p$ = amplitude of the wall-normal velocity perturbation in the porous layer

$\check{\mathbf{v}}$ = deviation velocity vector, i.e. $\mathbf{v} - \langle \mathbf{v} \rangle^f$

v_{max} = maximum allowed suction velocity

v_{min} = minimum allowed suction velocity

v_s = suction velocity

v_w = wall-normal perturbation velocity at the wall

$\langle \mathbf{v} \rangle$ = superficial volume-averaged velocity

$\langle \mathbf{v} \rangle^f$ = intrinsic volume-averaged velocity

$\langle v \rangle$ = non-dimensional volume-averaged wall-normal laminar flow velocity

V = non-dimensional wall-normal laminar flow velocity

$\mathcal{V}$ = spherical volume used in the volume averaging process

$\mathcal{V}_f$ = volume of fluid in the averaging volume $\mathcal{V}$

x, y, z = rectangular coordinates

Greek symbols

α = streamwise wavenumber

α_i = imaginary part of the streamwise wavenumber α

α_r = real part of the streamwise wavenumber α

β = spanwise wavenumber

δ_1 = boundary layer displacement thickness when permeability is nonzero

δ_{99} = boundary layer thickness when permeability is nonzero

ε = porosity

γ = $(1/\sqrt{\varepsilon}) - \tau$

κ = magnitude of the wave vector, $\sqrt{\alpha^2 + \beta^2}$

μ = fluid viscosity

ν = kinematic viscosity

ω = frequency

ρ = fluid density

σ = non-dimensional permeability

σ_{max} = maximum allowed non-dimensional permeability

σ_{min} = minimum allowed non-dimensional permeability

τ = fluid-porous interface coefficient

$\widetilde{\eta}$ = amplitude of the wall-normal vorticity perturbation

$\widetilde{\eta}_p$ = amplitude of the wall-normal vorticity perturbation in the porous layer

Subscripts

c = indicates critical Reynolds number

f = identifies a quantity associated with the fluid phase of the porous layer

i = indicates imaginary part

max = indicates maximum value allowed

min = indicates minimum value allowed

p = indicates flow quantities evaluate within the porous layer

r = indicates real part

s = suction flow quantities

sl = identifies a quantity associated with the solid phase of the porous layer

w = wall flow quantities

1 = indicates boundary layer displacement thickness

99 = indicates boundary layer thickness

∞ = flow quantities at infinity

Superscripts

T = transpose vector

$'$ = indicates d/dy

$''$ = indicates d^2/dy^2

I. Introduction

This study is motivated by the increasing use of porous surfaces for passive and active flow control in aerodynamic applications. Passive flow control using wall-suction, in which fluid is bled from a high-pressure region to a low-pressure region through a porous surface, has been investigated since the 1970's for a broad range of applications. These include the reduction of drag on bluff bodies [1], the reduction of shock-induced separation on transonic airfoils [2], laminar flow control [3], aerodynamic maneuver control of tailless fighter aircraft [4], the reduction of unsteady lift forces on airfoils [5], and the reduction of yawing moments on porous projectile forebodies [6, 7]. Efforts towards active flow control include the microfabrication of valve arrays [8, 9] to intelligently control wall suction. Success has been reported by integrating a self-actuated check valve into a small, thin-membrane, flapping wing [8]. Kearney and Glezer [10, 11] have also demonstrated that actively controlled suction distributed over a Clark-Y airfoil can beneficially alter aerodynamic forces and moments by modifying the airfoil's apparent aerodynamic shape.

Continuously distributed suction and injection of fluid through porous surfaces has also been widely investigated as a means of stabilizing boundary layers, attenuating wall turbulence and reducing skin friction drag in wall-bounded shear flows [12–14]. Most of these studies model wall suction and injection by prescribing a desired wall-normal velocity on the porous surface while also applying the no-slip condition. The validity of this approach is unclear because it neglects the flow occurring within the pores of the surface. Experimental [16, 17] and theoretical [17–20] studies of shear flows bounded by passive porous surfaces have shown that the fluid flow occurring within the pores of the surfaces tends to promote early transition to turbulence. This destabilizing effect can be dramatic, even when the permeability of the surface is small [18–20], and it appears to contradict the objective of attenuating wall turbulence using wall-transpiration. Existing models of flow control using wall-transpiration cannot consider this contradiction because they neglect the flow occurring within the porous material. This neglect may limit the accuracy of these control models, particularly because such models are usually based on the assumption that wall-bounded shear flows are sensitive to near-wall phenomena.

The current study shows that the stabilization of boundary layers by suction through a porous

surface is possible, but may not be as effective as predicted by classical stability analyses. To this end, we extend previous theoretical stability analyses of fully developed channel flows bounded by porous walls [17–19] to a new linear stability analysis of the asymptotic suction boundary layer (ASBL) [21]. The ASBL is the simplest example of a drag reduction method that uses wall suction to increase boundary layer stability. The ASBL forms through the application of uniform constant wall suction to a flat plate boundary layer with constant free-stream velocity, U_∞. Due to the suction, the boundary layer stops growing after a sufficient downstream distance from the leading edge, and is significantly more stable than a Blasius boundary layer [22]. The wall suction increases stability by reducing the boundary layer's thickness and by altering the laminar velocity profile such that less energy is transferred from the base-flow to disturbances. As a result, the ASBL has a critical Reynolds number around 54370 [23], which is two orders of magnitude greater than that for a Blasius boundary layer, which is around 520 [24]. Unless otherwise specified, the Reynolds number throughout this study is defined as $Re = \rho U_\infty \delta_1 / \mu$, where ρ and μ are the fluid density and viscosity, respectively, U_∞ is the free-stream velocity, and δ_1 is the boundary layer displacement thickness.

Experimentally, wall suction has been implemented using spanwise slots, discrete holes, and wholly porous materials. One advantage of applying suction through discrete holes is that a skin with discrete holes can continue to act as a continuous structural member [25]. The main disadvantage is that discrete holes can produce three-dimensional effects, such as streamwise vortices, that provoke early transition. MacManus and Eaton [26] have shown that discrete holes do not provoke early transition when the ratio of their diameter, $\mathcal{D}$, to the boundary layer's displacement thickness is less than 0.6, i.e. $\mathcal{D}/\delta_1 < 0.6$. Wholly porous materials are often used [27–29] because they provide a uniform suction velocity without provoking three-dimensional effects, and can be manufactured cheaply. In wind-tunnel experiments of a NACA 64A010 airfoil with a fully porous sintered bronze skin, Braslow *et al.* [30] observed full chord laminar flow up to a chord Reynolds number of 1.98×10^7. This corresponded to a net drag reduction of around 60 %. Reynolds and Saric [28] and Reed and Nayfeh [31] have also found that suction applied through wholly porous strips can be as effective as suction applied continuously over a much longer streamwise length. For discussion of the design

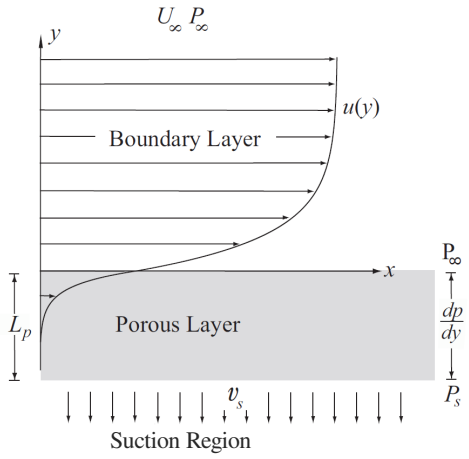

Fig. 1 Geometry and laminar velocity profile, not to scale, of the asymptotic suction boundary layer considered in the current study.

considerations of wall transpiration, we refer readers to references [12, 13, 27, 32–34].

Suction through a wholly porous layer is usually implemented experimentally by applying a pressure gradient to a layer of homogeneous porous material [22, 27, 29, 30], as illustrated in Fig. 1. The pressure gradient may be applied using a pump or by leveraging an existing pressure differential between the two sides of the porous layer. In contrast, previous theoretical studies of the ASBL model the effect of the porous layer on the laminar base-flow through a pair of boundary conditions. These are the prescription of the no-slip boundary condition as well as a desired wall-normal velocity, $v = -v_s$ where $v_s > 0$, on the porous surface. Linear stability analyses also assume that velocity perturbations vanish at the wall. These assumptions neglect the penetration of the base-flow and perturbations into the porous layer and underlying suction region. In the current study, we find these assumptions have a major impact on the stability of the ASBL at medium-high Reynolds numbers (i.e. $Re \sim 10^4$). For the limited range of low Reynolds numbers previously studied, $300 \leq Re \leq 1200$, however, there is generally good agreement between classical modelling and experimental studies [29, 35–39].

The geometry of the ASBL considered in the current study is shown in Fig. 1. We consider a fluid-saturated, homogeneous, isotropic, rigid, porous layer of thickness L_p at a zero angle of incidence. The porous layer is bounded above by a semi-infinite fluid region at constant pressure, P_∞, in which a boundary layer is driven by a constant free-stream velocity, U_∞. The porous layer is

bounded below by a semi-infinite fluid region maintained at a constant suction pressure, $P_s < P_\infty$. The pressure difference across the porous layer drives a wall-normal suction velocity, v_s. We refer to the regions above and below the porous layer as the "boundary layer region" and "suction region," respectively. Note that the streamwise laminar flow, $u(y)$, extends from the boundary layer region into the porous layer (see Fig. 1). We restrict our study to porous layers of sufficiently large thickness and sufficiently small permeability such that the laminar streamwise velocity, $u(y)$, decays to zero within the porous region. We model the flow in the porous layer using a volume-averaged approach developed by Whitaker [40] and Ochoa-Tapia and Whitaker [41]. Although, this model is most readily applicable to wholly porous materials, it can be easily extended to the case of densely packed discrete holes by considering an anisotropic porous layer with zero permeability in the directions tangential to the wall. We perform a fully coupled, three-dimensional, spatial, linear stability analysis of the laminar flow in the boundary layer, porous layer, and suction regions. Our results are most applicable to suction controlled boundary layers whose thickness is nearly constant, and for which the magnitude of the suction velocity is small with respect to the freestream velocity.

To put the model we use for the flow in the porous layer in perspective, we briefly outline previous pertinent work. In 1856, Darcy developed the first empirical law governing Stokes flow through porous media [42]. Beavers and Joseph [15] proposed the first interface condition coupling a laminar channel flow with an adjacent porous flow governed by Darcy's law. The condition results in a velocity discontinuity at the interface. Whitaker [40] analytically derived general porous flow equations by volume averaging the Navier–Stokes and continuity equations. Subsequently, Ochoa-Tapia and Whitaker [41, 43, 44] analytically derived interfacial momentum transfer conditions that couple a homogeneous fluid flow with an adjacent porous flow. Recently, these interface conditions have been further developed by Valdés-Parada and co-workers [45, 46]

To our knowledge, Beavers, Sparrow and Magnuson [16] were the first to experimentally investigate the destabilizing effects of wall permeability in channel flows. Subsequently, Sparrow *et al.* [17] experimentally investigated the critical Reynolds numbers for channels with one porous wall, and performed a two-dimensional linear stability analysis using Darcy's law with the Beavers and Joseph [15] interface condition. They found, both experimentally and numerically, that wall permeability

decreased the critical Reynolds number with respect to the value for a channel flow with impermeable walls. Tilton and Cortelezzi [18, 19] performed a three-dimensional linear stability analysis of channel flows with one or two porous walls using the governing equations of Whitaker [40] with the interface conditions of Ochoa-Tapia and Whitaker [41]. Their results are restricted to small permeabilities for which inertial effects in the porous regions can be neglected. They found that the overall stability of a channel flow with porous walls is dictated by several competing mechanisms. Briefly, the penetration of wall-normal velocity perturbations into the porous walls is destabilizing, while the presence of a wall-tangential interface velocity is stabilizing. In the majority of the parameter space explored, Tilton and Cortelezzi [19] found the destabilizing effects dominated.

The volume-averaged approach used in the current study helps address the broader issue of how to best model porous surfaces for boundary layer control. Previous studies have mainly investigated the stability of boundary layers over porous walls by assuming the wall-normal perturbation velocity passing through the porous wall, v_w, can be coupled to the perturbation pressure at the wall, p_w, by introducing the concept of an admittance f, such that $v_w = f\, p_w$ [3, 48, 49]. The no-slip condition is applied to the fluid velocity tangential to the wall, and the laminar base-state is unaffected by the porous surface. This approach has produced mixed results. Lekoudis [49] derived a relationship for f for the case of perforated plates. Unfortunately, several inconsistencies in his derivation limit the reliability of his results (see Tilton [20] for details). Subsequently, Carpenter and Porter [3] treated the admittance as a complex number that is prescribed. This, however, neglects the flow within the porous wall, and does not address the more fundamental question of how f could be determined for actual porous materials. To our knowledge, the volume-averaged approach considered in the current study has never been applied to wall-suction; however, the interface conditions of Ochoa-Tapia and Whitaker [41] have been successfully applied to investigate laminar boundary layers over permeable wedges in the absence of suction [47].

This article is organized in the following manner. In §II, we outline the governing equations. In §III, we derive a general analytic expression for the laminar profile and illustrate the effects of permeability on the boundary layer thickness and displacement thickness. In §IV, we non-dimensionalize the problem and derive the linear stability equations and interface conditions. In

§V, we present the linear stability results and compare our results with the experimental results of Fransson and Alfredsson [29]. We present our conclusions in §VI.

II. Governing Equations

The flow of an incompressible viscous fluid in the boundary layer and suction regions (see Fig. 1) is governed by the Navier–Stokes and continuity equations,

$$\rho\left(\frac{\partial \mathbf{v}}{\partial t} + \mathbf{v}\cdot\nabla\mathbf{v}\right) = -\nabla p + \mu\nabla^2\mathbf{v}, \tag{1}$$

$$\nabla\cdot\mathbf{v} = 0, \tag{2}$$

where $\mathbf{v} = [u\ v\ w]^T$, p, ρ, and μ, are the fluid velocity vector, pressure, density, and viscosity, respectively.

The fluid flow within the porous layer (see Fig. 1) is also governed by equations (1)–(2) with no-penetration and no-slip conditions at the fluid–solid interfaces of the medium. The resulting boundary value problem, however, is prohibitively difficult due to the complex boundary conditions. Figure 2 illustrates a general porous material in which the smallest length scales, l_f and l_{sl}, are on the order of an average pore and particle diameter, respectively. The largest characteristic length scale is the thickness of the porous layer, L_p. The method of volume averaging simplifies the problem by averaging equations (1) and (2) over a small spherical volume, V, of radius $r \ll L_p$. The length scales are assumed to be well separated, $l_{sl} \sim l_f \ll r \ll L_p$ [40]. Every point in a volume-averaged flow field has a volume-averaged velocity and pressure such that the porous medium is treated as a continuum. Two different averages are used [40]. The *superficial* volume average of some function, ψ, associated with the fluid is defined as

$$\langle\psi\rangle = \frac{1}{\mathcal{V}}\int_{\mathcal{V}_f} \psi\,\mathrm{d}\mathcal{V}_f,$$

and the *intrinsic* volume average is defined as

$$\langle\psi\rangle^f = \frac{1}{\mathcal{V}_f}\int_{\mathcal{V}_f} \psi\,\mathrm{d}\mathcal{V}_f,$$

where $\mathcal{V}_f < \mathcal{V}$ is the volume of fluid in the averaging volume, $\mathcal{V}$. The two averages are related by $\langle\psi\rangle = \varepsilon\langle\psi\rangle^f$, where $\varepsilon = \mathcal{V}_f/\mathcal{V}$ is the *porosity*.

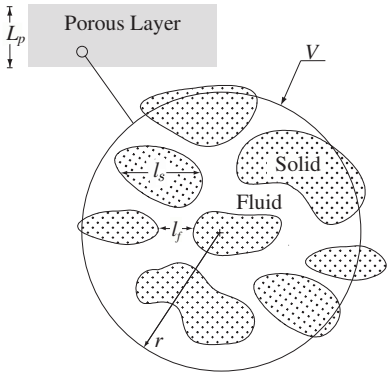

Fig. 2 Sketch of a porous medium with complicated fluid–solid interfaces. Not to scale

The volume-averaged Navier–Stokes and continuity equations derived by [40] for an incompressible viscous fluid flowing through a rigid, homogeneous, isotropic, porous medium are

$$\frac{\rho}{\varepsilon}\left(\frac{\partial\langle\mathbf{v}\rangle}{\partial t}+\frac{\langle\mathbf{v}\rangle\cdot\nabla\langle\mathbf{v}\rangle}{\varepsilon}+\nabla\cdot\langle\check{\mathbf{v}}\check{\mathbf{v}}\rangle\right)=-\nabla\langle p\rangle^{f}+\frac{\mu}{\varepsilon}\nabla^{2}\langle\mathbf{v}\rangle-\frac{\mu}{k}\langle\mathbf{v}\rangle-\frac{\mu}{k}\mathbf{F}\cdot\langle\mathbf{v}\rangle, \tag{3}$$

$$\nabla\cdot\langle\mathbf{v}\rangle=0. \tag{4}$$

The superficial volume-averaged velocity, $\langle\mathbf{v}\rangle$, is the preferred representation of the velocity because it is always solenoidal. For the pressure, the intrinsic volume average, $\langle p\rangle^{f}$, is preferred because it is the pressure measured by a probe in an experimental apparatus. The permeability, $k\geq 0$, measures the resistance to fluid flow. If $k=0$, the medium is impermeable. In equation (3), the Darcy term, $\mu\langle\mathbf{v}\rangle/k$, represents a volume-averaged viscous drag, while the Forchheimer term, $\mu\mathbf{F}\cdot\langle\mathbf{v}\rangle/k$, where $\mathbf{F}$ is a second-order tensor, represents a drag due to inertial effects. The tensor $\mathbf{F}$ depends on the structure of the porous medium. Experimentally it is often found to be a linear function of the volume-averaged velocity, $\langle\mathbf{v}\rangle$, [40]. The deviation velocity, $\check{\mathbf{v}}=\mathbf{v}-\langle\mathbf{v}\rangle^{f}$, is the difference between the velocity, $\mathbf{v}$, and the intrinsic volume-averaged velocity, $\langle\mathbf{v}\rangle^{f}$. It is important to note that volume averaging the convective term, $\rho(\mathbf{v}\cdot\nabla\mathbf{v})$, in the Navier–Stokes equation (1) generates the terms $\rho(\langle\mathbf{v}\rangle\cdot\nabla\langle\mathbf{v}\rangle)/\varepsilon^{2}$, $\rho(\nabla\cdot\langle\check{\mathbf{v}}\check{\mathbf{v}}\rangle)/\varepsilon$, and $\mu\mathbf{F}\cdot\langle\mathbf{v}\rangle/k$ in equation (3).

The adjacent fluid flows in the boundary layer region, porous layer, and suction region are coupled at $y=0$ and $y=-L_p$ using momentum transfer conditions derived by Ochoa-Tapia and Whitaker [41, 43, 44]. When inertial effects are non-negligible in the porous layer, these conditions are quite complex and involve a vector and fourth-order tensor that must be determined experi-

mentally [44]. Because there are currently no published data for these quantities, we restrict our analysis to flows for which the inertial effects can be ignored in the porous layer. This also allows us to neglect the convective terms $\rho(\langle \mathbf{v} \rangle \cdot \nabla \langle \mathbf{v} \rangle)/\varepsilon^2$, $\rho(\nabla \cdot \langle \check{\mathbf{v}} \check{\mathbf{v}} \rangle)/\varepsilon$, and $\mu \mathbf{F} \cdot \langle \mathbf{v} \rangle / k$ in equation (3). This assumption is only valid for porous media of small permeability in which the flow velocities are small with respect to the characteristic velocity in the purely fluid regions. The convective effects become negligible because the dense structures of the porous matrix impede motion between layers of fluid. We thus limit our study to permeabilities for which the fluid velocity in the porous region is much smaller than the free-stream velocity, $\langle \mathbf{v} \rangle \ll U_\infty$. Following this assumption, the temporal term, $\rho(\partial \langle \mathbf{v} \rangle / \partial t)/\varepsilon$, in equation (3) is likely small compared to the Darcy term [17, 40]. However, we retain it because we expect the unsteady effects of the purely fluid regions to penetrate slightly into the porous layer.

The governing equations (3)-(4) for the porous layer reduce to

$$\frac{\rho}{\varepsilon} \frac{\partial \langle \mathbf{v} \rangle}{\partial t} = -\nabla \langle p \rangle^f + \frac{\mu}{\varepsilon} \nabla^2 \langle \mathbf{v} \rangle - \frac{\mu}{k} \langle \mathbf{v} \rangle, \tag{5}$$

$$\nabla \cdot \langle \mathbf{v} \rangle = 0. \tag{6}$$

The momentum transfer conditions at $y = 0$ and $-L_p$ are

$$\mathbf{v} = \langle \mathbf{v} \rangle, \qquad p = \langle p \rangle^f, \tag{7}$$

$$\frac{1}{\varepsilon} \frac{\partial \langle u \rangle}{\partial y} - \frac{\partial u}{\partial y} = \pm \frac{\tau u}{\sqrt{k}}, \qquad \frac{1}{\varepsilon} \frac{\partial \langle w \rangle}{\partial y} - \frac{\partial w}{\partial y} = \pm \frac{\tau w}{\sqrt{k}}. \tag{8}$$

Note from (7)–(8) that the velocity and pressure at an interface are continuous, while the shear stress has a jump proportional to the interface coefficient τ which accounts for the distribution of momentum at the interface [41, 43]. The coefficient τ depends on a porous material's structure as well as the surface machining of the interface and must usually be determined experimentally. In a comparison with experiments, Ochoa-Tapia and Whitaker [43] found that τ varied roughly between -1.0 and 1.5 and can also be zero (Brinkman's condition). When applying conditions (8) at the lower interface, $y = -L_p$, a negative sign precedes τ because the normal vector is defined as pointing into the purely fluid region. Hereinafter, we use the symbol $\pm$ to indicate that a positive sign is

used at the upper interface, $y = 0$, and a negative sign is used at the lower interface, $y = -L_p$. The converse is true of the symbol $\mp$.

III. Laminar Velocity Profile

In this section, we explore the effects of wall permeability on the fully developed laminar velocity profile of the ASBL. We assume the free-stream velocity, U_∞, free-stream pressure, P_∞, and the suction pressure, P_s, are all constant, see Fig. 1. Suction is applied from the leading edge of the plate onwards. After a sufficient downstream distance, the fully developed laminar velocity profile is a function of the wall-normal coordinate, y, only. Equations (1)–(2) governing the boundary layer region, $y \geq 0$, and suction region, $y \leq -L_p$, simplify to

$$v\frac{\mathrm{d}u}{\mathrm{d}y} = \nu\frac{\mathrm{d}^2u}{\mathrm{d}y^2}, \qquad p = \begin{cases} P_\infty, & y \geq 0 \\ P_s, & y \leq -L_p \end{cases}, \tag{9}$$

where v is constant. In the porous region, equations (5)–(6) simplify to

$$\langle u\rangle = \frac{k}{\varepsilon}\frac{\mathrm{d}^2\langle u\rangle}{\mathrm{d}y^2}, \qquad \langle v\rangle = -\frac{k}{\mu}\frac{\mathrm{d}\langle p\rangle^f}{\mathrm{d}y}, \tag{10}$$

where $\mathrm{d}\langle p\rangle^f/\mathrm{d}y = (P_\infty - P_s)/L_p$ is a positive constant. The adjacent flows are coupled by the momentum transfer conditions at $y = 0$ and $y = -L_p$,

$$u = \langle u\rangle, \qquad v = \langle v\rangle, \qquad \frac{1}{\varepsilon}\frac{\mathrm{d}\langle u\rangle}{\mathrm{d}y} - \frac{\mathrm{d}u}{\mathrm{d}y} = \pm\frac{\tau u}{\sqrt{k}}. \tag{11}$$

In the boundary layer region, we apply the freestream condition $u \to \infty$ as $y \to \infty$. In the suction region, we require u to remain bounded as $y \to \infty$.

We find the following solution to equations (9)–(11),

$$u = U_\infty + \left[H\left(1 + Ae^{-2L_p\sqrt{\varepsilon/k}}\right) - U_\infty\right]e^{-yv_s/\nu}, \quad v = -v_s, \qquad y \geq 0, \tag{12}$$

$$\langle u\rangle = H\left[e^{y\sqrt{\varepsilon/k}} + Ae^{(-2L_p-y)\sqrt{\varepsilon/k}}\right], \qquad \langle v\rangle = -v_s, \qquad -L_p \leq y \leq 0, \tag{13}$$

$$u = \frac{2H}{1-\tau\sqrt{\varepsilon}}e^{-L_p\sqrt{\varepsilon/k}}, \qquad v = -v_s, \qquad y \leq -L_p, \tag{14}$$

where

$$H = \frac{v_sU_\infty}{\nu}\left[\frac{1}{\sqrt{k\varepsilon}} + \frac{v_s}{\nu} - \frac{\tau}{\sqrt{k}} - \left(\frac{1}{\sqrt{k\varepsilon}} - \frac{v_s}{\nu} + \frac{\tau}{\sqrt{k}}\right)Ae^{-2L_p\sqrt{\varepsilon/k}}\right]^{-1}, \quad A = \frac{1+\tau\sqrt{\varepsilon}}{1-\tau\sqrt{\varepsilon}},$$

and $v_s = k(\mathrm{d}\langle p\rangle^f/\mathrm{d}y)/\mu$ is the magnitude of the wall suction. In the current study, we consider values of L_p, k, and ε such that $\exp(-L_p\sqrt{\varepsilon/k})$ is always less than 10^{-100}. Consequently, equations (12)–(14) simplify to

$$u = U_\infty\left(1 - \frac{\gamma\nu}{\gamma\nu + v_s\sqrt{k}}\mathrm{e}^{-yv_s/\nu}\right), \qquad v = -v_s, \qquad y \geq 0, \tag{15}$$

$$\langle u\rangle = U_\infty\left(\frac{v_s\sqrt{k}}{\gamma\nu + v_s\sqrt{k}}\right)\mathrm{e}^{y\sqrt{\varepsilon/k}}, \qquad \langle v\rangle = -v_s, \qquad -L_p \leq y \leq 0, \tag{16}$$

$$u = 0, \qquad v = -v_s, \qquad y \leq 0, \tag{17}$$

where $\gamma = (1/\sqrt{\varepsilon}) - \tau$.

When the permeability tends to zero, $k \to 0$, equations (15)–(17) reduce to the following solution used in all previous studies of the ASBL,

$$u = U_\infty\left(1 - \mathrm{e}^{-yv_s/\nu}\right), \qquad v = -v_s, \qquad y \geq 0. \tag{18}$$

In this case, an infinite pressure gradient, $\mathrm{d}\langle p\rangle^f/\mathrm{d}y$, is necessary to provide a finite suction velocity, v_s. The laminar velocity profile (18) has a displacement thickness $d_1 = \nu/v_s$, and a boundary layer thickness $d_{99} = d_1\ln(100)$. We reserve the symbols d_1 and d_{99} to represent the displacement thickness and boundary layer thickness, respectively, when the permeability is zero, $k = 0$.

To investigate the effects of permeability on the laminar velocity profile (15)–(17), we non-dimensionalize it using the characteristic length scale $d_1 = \nu/v_s$ and the characteristic time d_1/U_∞, obtaining

$$U = \frac{u}{U_\infty} = 1 - \frac{\gamma}{\gamma+\sigma}\mathrm{e}^{-y/d_1}, \qquad V = \frac{v}{U_\infty} = -\frac{1}{Re}, \qquad \frac{y}{d_1} \geq 0, \tag{19}$$

$$\langle U\rangle = \frac{\langle u\rangle}{U_\infty} = \frac{\sigma}{\gamma+\sigma}\mathrm{e}^{(y/d_1)\sqrt{\varepsilon}/\sigma}, \qquad \langle V\rangle = \frac{\langle v\rangle}{U_\infty} = -\frac{1}{Re}, \qquad -\frac{L_p}{d_1} \leq \frac{y}{d_1} \leq 0, \tag{20}$$

$$U = 0, \qquad V = -\frac{1}{Re}, \qquad \frac{y}{d_1} \leq -\frac{L_p}{d_1}, \tag{21}$$

where $Re = U_\infty d_1/\nu = U_\infty/v_s$, and $\sigma = \sqrt{k}/d_1$ is the non-dimensional permeability that may be interpreted as the ratio between a length scale characterizing the permeable material, $\sqrt{k}$, and

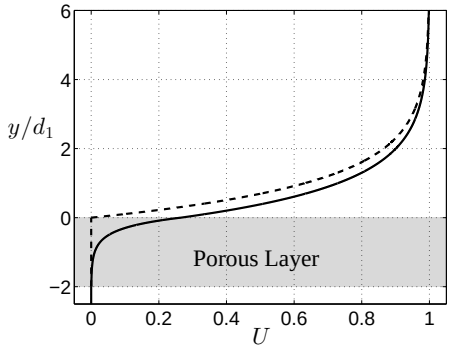

Fig. 3 The streamwise laminar velocity profile of the ASBL using the parameters $L_p = 2d_1$, $\varepsilon = 0.95$, $\tau = 0.194$, $\sigma = 0$ (dashed line) and $\sigma = 0.3$ (solid line).

a length scale characterizing the boundary layer thickness [15]. We use capital italics to represent the non-dimensionalized laminar flow in the purely fluid regions, $[U \;\; V \;\; 0]^T$, and porous layer, $[\langle U \rangle \;\; \langle V \rangle \;\; 0]^T$.

The dashed line in Fig. 3 illustrates the profile of the laminar streamwise velocity of the ASBL, when $\sigma = 0$. The streamwise velocity is zero for $y \leq 0$. The solid line illustrates the profile when $\varepsilon = 0.95$, $\tau = 0.194$, and $\sigma = 0.3$. These values correspond to Foametal, a porous material used in experiments by Beavers and Joseph [15]. The non-dimensional permeability, σ, is set to a large value for illustration purposes. Due to the non-zero permeability, there is a streamwise laminar velocity at the porous interface, $y = 0$, that decays monotonically within the porous layer. As a result, the displacement thickness, δ_1, and boundary layer thickness, δ_{99}, of the laminar velocity profile (15) decrease and can be expressed in terms of d_1 and σ as

$$\delta_1 = d_1 \frac{\gamma}{\gamma + \sigma}, \qquad \delta_{99} = d_1 \ln\left(100 \frac{\gamma}{\gamma + \sigma}\right). \tag{22}$$

We reserve the symbols δ_1 and δ_{99} to represent the displacement thickness and boundary layer thickness, respectively, when the permeability is nonzero, $\sigma \neq 0$. Note that δ_1 and δ_{99} are independent of U_∞ in an ASBL. In an experiment, δ_1 and δ_{99} can be varied by changing the suction velocity, v_s. For a fixed suction velocity, v_s, the Reynolds number, $Re = U_\infty / v_s$, can be varied by changing the free-stream velocity, U_∞.

IV. The Fully Coupled Linear Stability Problem

Consistent with previous studies and with the non-dimensionalization of the laminar velocity profile (19)–(21), we non-dimensionalize the governing equations (1)–(2) and (5)–(6) and interface conditions (7)–(8) using the characteristic length, $d_1 = \nu/v_s$, and characteristic time, d_1/U_∞. We define the non-dimensional pressure as $p/\rho U_\infty^2$. All subsequent equations and parameters are non-dimensional except when explicitly noted. We refer to the non-dimensional thickness of the porous layer as L_p. The non-dimensional governing equations in the boundary layer and suction regions are

$$\frac{\partial \mathbf{v}}{\partial t} + \mathbf{v}\cdot\nabla\mathbf{v} = -\nabla p + \frac{1}{Re}\nabla^2\mathbf{v}, \qquad \nabla\cdot\mathbf{v} = 0, \tag{23}$$

while the non-dimensional governing equations in the porous layer are

$$\frac{1}{\varepsilon}\frac{\partial\langle\mathbf{v}\rangle}{\partial t} = -\nabla\langle p\rangle^f + \frac{\nabla^2\langle\mathbf{v}\rangle}{\varepsilon Re} - \frac{\langle\mathbf{v}\rangle}{\sigma^2 Re}, \qquad \nabla\cdot\langle\mathbf{v}\rangle = 0. \tag{24}$$

The non-dimensional momentum transfer conditions at $y = 0$ and $y = -L_p$ are

$$\mathbf{v} = \langle\mathbf{v}\rangle, \qquad p = \langle p\rangle^f, \tag{25}$$

$$\frac{\sigma}{\varepsilon}\frac{\partial\langle u\rangle}{\partial y} - \sigma\frac{\partial u}{\partial y} = \pm\tau u, \qquad \frac{\sigma}{\varepsilon}\frac{\partial\langle w\rangle}{\partial y} - \sigma\frac{\partial w}{\partial y} = \pm\tau w. \tag{26}$$

We analyze the stability of the fully developed laminar flow in the boundary layer and suction regions with respect to small planar wave perturbations, $\hat{\mathbf{v}} = [\hat{u}\ \hat{v}\ \hat{w}]^T$ and $\hat{p}$, of the form

$$\begin{pmatrix} \hat{\mathbf{v}} \\ \hat{p} \end{pmatrix} = \begin{pmatrix} \widetilde{\mathbf{v}}(y) \\ \widetilde{p}(y) \end{pmatrix} \mathrm{e}^{\mathrm{i}(\alpha x + \beta z - \alpha c t)}, \tag{27}$$

where $\mathrm{i} = \sqrt{-1}$. The perturbations $\hat{\mathbf{v}}$ and $\hat{p}$ travel in the direction $(\alpha, 0, \beta)$ with streamwise and spanwise wavenumbers α and β, respectively, a phase speed c, a frequency $\omega = \alpha c$, and a wall-normal structure prescribed by $\widetilde{\mathbf{v}}(y)$ and $\widetilde{p}(y)$. We consider a spatial analysis for which ω and β are real, while $\alpha = \alpha_r + \mathrm{i}\alpha_i$, $\widetilde{\mathbf{v}}(y)$ and $\widetilde{p}(y)$, are generally complex. Assuming $x > 0$, a velocity perturbation,

$$\hat{\mathbf{v}}(x, y, z, t) = \widetilde{\mathbf{v}}(y)\mathrm{e}^{-\alpha_i x} e^{\mathrm{i}(\alpha_r x + \beta z - \omega t)},$$

is unstable if $\alpha_i < 0$. As will be shown later, the spatial approach used here is more complicated than a temporal linear stability analysis because the spatial approach produces a nonlinear eigenvalue

problem for α. Increasingly, current studies prefer the spatial approach because it corresponds more closely to experiments in which a disturbance is introduced at an upstream location and develops spatially as it flows downstream.

The linear stability equations for the boundary layer and suction regions are obtained by substituting $\mathbf{v} = [U + \hat{u} \;\; V + \hat{v} \;\; \hat{w}]^T$ and $p = P + \hat{p}$, into equations (23) and linearizing. Equation (27) is then used to obtain the following linear stability equations

$$\left[(\alpha U - \alpha c - \mathrm{i}V\mathrm{D}) \left(\mathrm{D}^2 - \kappa^2\right) - \alpha U'' - \frac{1}{\mathrm{i}Re} \left(\mathrm{D}^2 - \kappa^2\right)^2 \right] \widetilde{v}(y) = 0, \tag{28}$$

$$\left[(\alpha U - \alpha c - \mathrm{i}V\mathrm{D}) - \frac{1}{\mathrm{i}Re} \left(\mathrm{D}^2 - \kappa^2\right) \right] \widetilde{\eta}(y) = -\beta U' \widetilde{v}, \tag{29}$$

where a prime and D both denote $\mathrm{d}/\mathrm{d}y$, $\kappa = \sqrt{\alpha^2 + \beta^2}$, $\widetilde{v}$ is the amplitude of the wall-normal velocity perturbation, and $\widetilde{\eta} = \partial\widetilde{u}/\partial z - \partial\widetilde{w}/\partial x$ is the amplitude of the wall-normal vorticity perturbation, respectively. Equations (28) and (29) are modified forms of the Orr-Sommerfeld and Squire equations, respectively, with added terms to account for the wall-normal laminar flow, V. Throughout our study, we simply refer to equations (28) and (29) as the Orr-Sommerfeld and Squire equations, respectively.

We assume that perturbations in the porous layer have wave-like forms given by

$$\begin{pmatrix} \langle \hat{\mathbf{v}} \rangle \\ \langle \hat{p} \rangle^f \end{pmatrix} = \begin{pmatrix} \widetilde{\mathbf{v}}_p(y) \\ \widetilde{p}_p(y) \end{pmatrix} \mathrm{e}^{\mathrm{i}(\alpha x + \beta z - \alpha c t)}, \tag{30}$$

so that perturbations in the porous layer have identical wavenumbers and phase speeds as perturbations in the purely fluid regions. The linear stability equations for the porous region are obtained by substituting expressions (30) into equations (24) and rearranging the resulting equations for $\widetilde{\mathbf{v}}_p(y)$ and $\widetilde{p}_p(y)$ into the following counterparts to the Orr-Sommerfeld and Squire equations

$$\left[-c \left(\mathrm{D}^2 - \kappa^2\right) - \frac{1}{\mathrm{i}\alpha Re} \left(\mathrm{D}^2 - \kappa^2\right)^2 + \frac{\varepsilon}{\mathrm{i}\alpha\sigma^2 Re} \left(\mathrm{D}^2 - \kappa^2\right) \right] \widetilde{v}_p(y) = 0, \tag{31}$$

$$\left[-c - \frac{1}{\mathrm{i}\alpha Re} \left(\mathrm{D}^2 - \kappa^2\right) + \frac{\varepsilon}{\mathrm{i}\alpha\sigma^2 Re} \right] \widetilde{\eta}_p(y) = 0, \tag{32}$$

where $\widetilde{v}_p$ and $\widetilde{\eta}_p$ are the amplitudes of the wall-normal velocity and vorticity perturbations, respectively, in the porous layer. Because inertial effects have been neglected in the porous layer, equations

(31)–(32) lack any term directly coupling the disturbances in the porous layer with the laminar velocity in the porous layer. For the same reason, equation (32) is homogeneous unlike the Squire equation (29). However, the stability equations (31) and (32) have new terms, $\varepsilon\left(\mathrm{D}^2-\kappa^2\right)/\mathrm{i}\alpha\sigma^2 Re$ and $\varepsilon/\mathrm{i}\alpha\sigma^2 Re$, respectively, arising from the Darcy drag term.

The current study is mainly interested in the least stable eigenmode, called the Tollmien-Schlichting wave, because it determines the critical Reynolds number. Because the Tollmien-Schlichting wave vanishes in the far-stream [50, 51], we apply the far-stream boundary conditions,

$$\widetilde{\eta}\Big|_{y\to\infty} = \widetilde{v}\Big|_{y\to\infty} = \frac{\mathrm{d}\widetilde{v}}{\mathrm{d}y}\Big|_{y\to\infty} = 0, \tag{33}$$

We impose similar boundary conditions in the suction region,

$$\widetilde{\eta}\Big|_{y\to-\infty} = \widetilde{v}\Big|_{y\to-\infty} = \frac{\mathrm{d}\widetilde{v}}{\mathrm{d}y}\Big|_{y\to-\infty} = 0. \tag{34}$$

Using the momentum transfer conditions (25)–(26), we derive the following coupling conditions at the interfaces $y=0$ and $y=-L_p$,

$$\widetilde{v}=\widetilde{v}_p, \qquad \frac{\mathrm{d}\widetilde{v}}{\mathrm{d}y}=\frac{\mathrm{d}\widetilde{v}_p}{\mathrm{d}y}, \qquad -\frac{\sigma}{\varepsilon}\frac{\mathrm{d}^2\widetilde{v}_p}{\mathrm{d}y^2}+\sigma\frac{\mathrm{d}^2\widetilde{v}}{\mathrm{d}y^2}=\mp\tau\frac{\mathrm{d}\widetilde{v}}{\mathrm{d}y}, \tag{35}$$

$$\begin{aligned}&\frac{1}{\varepsilon Re}\frac{\mathrm{d}^3\widetilde{v}_p}{\mathrm{d}y^3}-\frac{1}{Re}\frac{\mathrm{d}^3\widetilde{v}}{\mathrm{d}y^3}-i\alpha U'\tilde{v}+V\frac{\mathrm{d}^2\widetilde{v}}{\mathrm{d}y^2}\\ &+\left[\left(\frac{1}{\varepsilon}-1\right)\left(\mathrm{i}\alpha c-\frac{\kappa^2}{Re}\right)-\frac{1}{\sigma^2 Re}+\mathrm{i}\alpha U\right]\frac{\mathrm{d}\widetilde{v}}{\mathrm{d}y}=0,\end{aligned} \tag{36}$$

$$\widetilde{\eta}=\widetilde{\eta}_p, \qquad \frac{\sigma}{\varepsilon}\frac{\mathrm{d}\widetilde{\eta}_p}{\mathrm{d}y}-\sigma\frac{\mathrm{d}\widetilde{\eta}}{\mathrm{d}y}=\pm\tau\widetilde{\eta}. \tag{37}$$

For a given combination of ω, β, and Re, equations (28)–(29) and (31)–(32), coupled with the appropriate interface and boundary conditions (33)–(37), pose an eigenvalue problem for the eigenvalue α and eigenfunctions $\widetilde{v}$ and $\widetilde{\eta}$. The eigenmodes can be separated into two complementary sets. The eigenmodes found by solving the coupled equations (28) and (31) are referred to as the Orr-Sommerfeld modes [19, 52]. When $\widetilde{v}=0$, the coupled equations (29) and (32) produce a second set modes referred to as the Squire modes.

We solve the fully coupled linear stability problem using the Chebyshev spectral method described in detail by [19] and [20]. We find that the required number of Chebyshev polynomials increases as the permeability, σ, decreases. For this reason, we set the minimum allowable permeability to $\sigma_{min}=0.0001$.

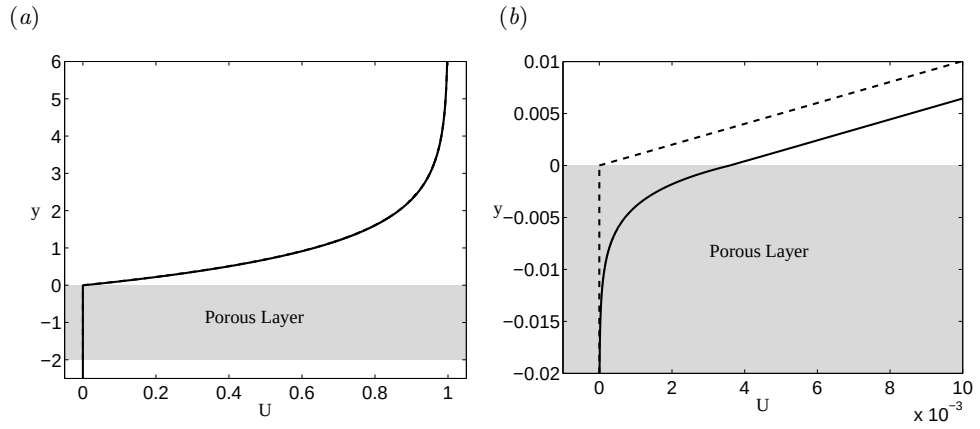

Fig. 4 The laminar velocity profiles for $L_p = 2$, $\varepsilon = 0.95$, $\tau = 0.194$, $\sigma = 0$ (dashed line) and $\sigma = 0.003$ (solid line): (a) full view; (b) magnified view at the interface $y = 0$. The porous region is shaded grey.

V. Results

We perform a series of numerical experiments in which we fix the porosity, $\varepsilon = 0.95$, and interface coefficient, $\tau = 0.194$, so the porous layer behaves like Foametal [15]. We choose this material because Tilton and Cortelezzi [19] found it affects the stability of channel flows in a qualitatively similar manner to a wide range of porous materials. We vary the non-dimensional permeability, σ, between $\sigma_{min} = 0.0001$ and $\sigma_{max} = 0.003$. This procedure is similar to a laboratory experiment in which $\sigma = \sqrt{k}v_s/\nu$ is varied by changing the suction velocity. In a laboratory experiment, the non-dimensional thickness of the porous layer, L_p, also varies with v_s. In our numerical experiment, however, the number of Chebyshev polynomials necessary for the numerical solution increases significantly as L_p increases [20]. For numerical convenience, we fix L_p and vary only σ. We begin by characterizing our results when $L_p = 2$, and then repeat our computations using $L_p = 4$, 6, and 8.

Tilton and Cortelezzi [19] found that inertial effects in the momentum transfer conditions of Ochoa-Tapia and Whitaker [44] increase with the product of the laminar interface velocity, non-dimensional permeability, and Reynolds number, i.e. $U(0)\sigma Re$. We perform a similar analysis and estimate that inertial effects are negligible below $\sigma_{max} = 0.003$ when $\varepsilon = 0.95$, $\tau = 0.194$, and $L_p \leq 8$ [20]. Figure 4(a) illustrates the laminar velocity profiles for $\sigma_{max} = 0.003$ (solid line) and $\sigma = 0$ (dashed line). Though the profiles appear indistinguishable, the magnified view in Fig. 4(b)

demonstrates a small laminar interface velocity of $U(0) = 0.359\ \%\ U_\infty$ when $\sigma = \sigma_{max}$.

We compare our stability results for $0.0001 \leq \sigma \leq 0.003$, with the results of a linear stability analysis that neglects the effects of wall-permeability. These are computed, as in all previous studies, by substituting $\sigma = 0$ into equations (19)–(21) and solving the stability equations (28)–(29) with the boundary conditions $\widetilde{\eta} = \widetilde{v} = \mathrm{D}\widetilde{v} = 0$ at $y = 0$, and the far-stream conditions (33). We validate our results for $\sigma = 0$ by comparison with previously published studies. We validate results for finite permeabilities, $0.0001 \leq \sigma \leq 0.003$, by verifying that our results for $\sigma_{min} = 0.0001$ approach the results for $\sigma = 0$, and by comparison with the experimental results of Fransson and Alfredsson [29].

A. Effects of Wall Permeability on the Tollmien-Schlichting Wave

The Orr-Sommerfeld and Squire spectra of the ASBL are composed of several continuous spectra and a small number of discrete modes [20, 52]. We find that wall permeability destabilizes neither the Squire modes nor the continuous spectra, but significantly destabilizes the discrete Orr-Sommerfeld mode known as the Tollmien-Schlichting (TS) wave (consistent with [19]). Furthermore, we find that Squire's theorem [52] remains valid such that the stability of the TS wave is minimized for two-dimensional perturbations with a spanwise wavenumber of zero, $\beta = 0$.

The solid line in Fig. 5(a) illustrates the trajectory of the complex eigenvalue, $\alpha = \alpha_r + \mathrm{i}\alpha_i$, associated with the TS wave as the permeability increases from $\sigma_{min} = 0.0001$ to $\sigma_{max} = 0.003$ for the constant parameters $L_p = 2$, $F = 0.803805$, $\beta = 0$, and $Re = 40000$. To be consistent with previous spatial linear stability analyses, we use the non-dimensional frequency $F = 10^6\omega/Re$ [52]. The trajectory is generated using $F = 0.830805$ to facilitate comparison with the temporal linear stability results of Tilton [20]. The dash-dotted line marks the real axis, $\alpha_i = 0$, and the circle centered at $\alpha = 0.1994$+i0.002997 shows the complex wavenumber of the TS wave for the case $\sigma = 0$. At $\sigma_{min} = 0.0001$, the TS wave is stable and has the complex wave number $\alpha = 0.1994 + \mathrm{i}0.002939$ that agrees with the result for $\sigma = 0$ up to four decimal places. Recall that a perturbation is unstable when $\alpha_i < 0$. When $\sigma = 0.00071$, the TS wave is neutrally stable, $\alpha_i = 0$, and has the real wavenumber $\alpha = 0.2$. When $\sigma = 0.003$, the wave is unstable and has the complex wave number $\alpha = 0.1908 - \mathrm{i}0.05526$.

Figure 5(b), illustrates the eigenfunctions $\widetilde{v}(y)$ (solid line) and $\widetilde{p}(y)$ (dashed line) of the TS

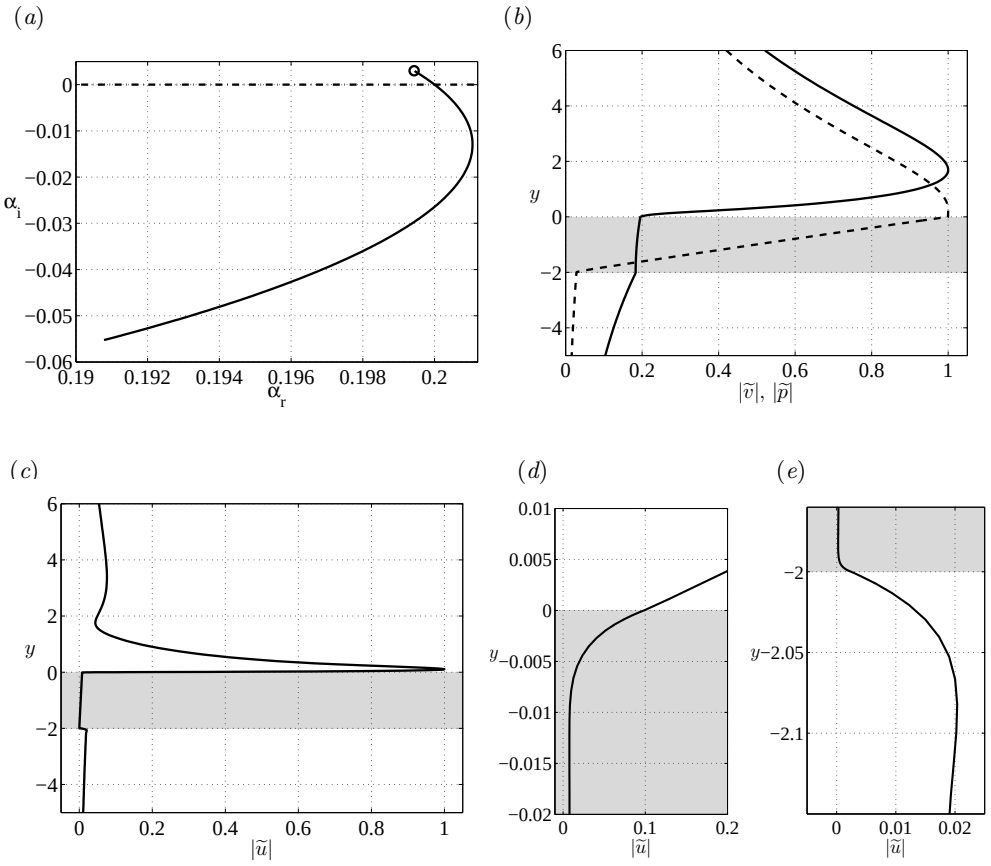

Fig. 5 Effects of wall permeability on the TS wave when $L_p = 2$, $\beta = 0$, $F = 0.803805$, and $Re = 40000$. (a) Trajectory of the complex eigenvalue, $\alpha = \alpha_r + \mathrm{i}\alpha_i$, as σ increases from $\sigma_{min} = 0.0001$ to $\sigma_{max} = 0.003$. The eigenvalue for the case $\sigma = 0$ is circled. The real axis, $\alpha_i = 0$, is represented as a dash-dotted line. (b) The eigenfunction magnitudes $|\widetilde{v}|$ (solid line) and $|\widetilde{p}|$ (dashed line) at $\sigma_{max} = 0.003$. The porous region is shaded grey. (c) The eigenfunction magnitude $|\widetilde{u}|$ (solid line) at $\sigma_{max} = 0.003$. (d) Magnified view of $|\widetilde{u}|$ at the upper interface $y = 0$. (e) Magnified view of $|\widetilde{u}|$ at the lower interface $y = -2$.

wave in Fig. 5(a) at $\sigma_{max} = 0.003$. For brevity, only the magnitudes, $|\widetilde{v}(y)|$ and $|\widetilde{p}(y)|$, of the complex eigenfunctions are shown. Hereinafter, all eigenfunctions are scaled so their maxima equal unity. We observe that the wall-normal velocity of the TS wave has a significant magnitude, $|\widetilde{v}|$, throughout the porous layer and vanishes asymptotically in the far-stream, $y \to \infty$, and far suction region, $y \to -\infty$. The wall-normal perturbation velocity in the porous layer is likely driven by the perturbation pressure whose magnitude, $|\widetilde{p}|$, has a maximum at $y = 0$ and a nearly linear drop, $d|\widetilde{p}|/dy$, across the porous layer. Figure 5(c) illustrates the eigenfunction $|\widetilde{u}|$ describing the

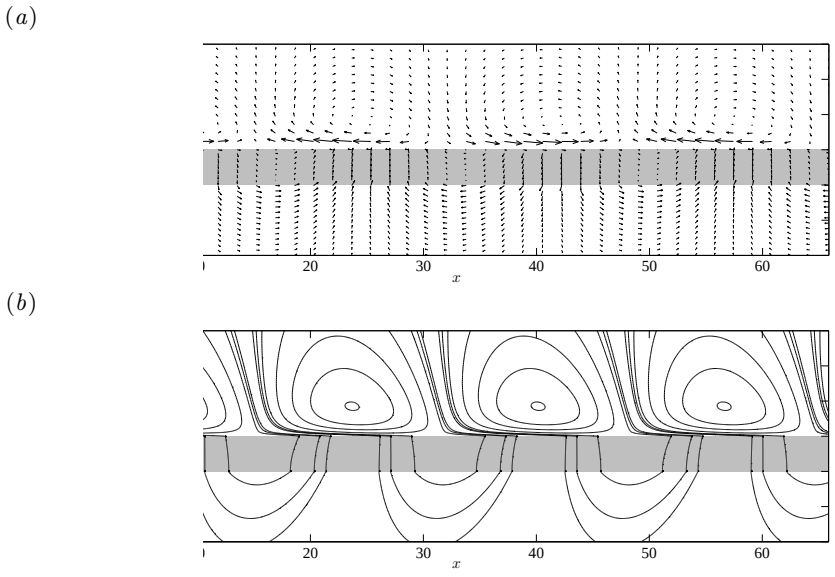

Fig. 6 Velocity vectors (panel *a*) and streamlines (panel *b*) produced by the TS eigenfunctions $\widetilde{u}$ and $\widetilde{v}$ when $L_p=2$, $\beta=0$, $F=0.803805$, $Re=40000$, and $\sigma = 0.003$. In both panels, the range of the x-axis covers two wavelengths, i.e. $0 \leq x \leq 4\pi/\alpha_r$. In panel (*a*), the arrows representing the velocity vectors have been scaled up for $y < 0$, in comparison to the scaling for $y > 0$, to aid in visualization.

streamwise velocity of the TS wave when $\sigma = \sigma_{max}$. Figures 5(d) and 5(e) show magnifications of $|\widetilde{u}|$ at the upper ($y=0$) and lower ($y=-2$) fluid-porous interfaces, respectively. From Fig. 5(d), we observe that $|\widetilde{u}|$ decreases rapidly from $|\widetilde{u}| = 0.098$ at $y=0$ to less than 0.008 at $y = -0.015$. This rapid decrease in $|\widetilde{u}|$ adjacent to the upper interface is qualitatively similar to the rapid decrease in the laminar streamwise velocity, U, illustrated in Fig. 4(b). In the porous flow community, these boundary layer type structures at the interface between a porous region and purely fluid region are called transition layers or *Brinkman layers*. Brinkman layers play an important role in the momentum transfer process at an interface and have received considerable attention in the literature [53]. Figure 5(e) illustrates a similar Brinkman layer at $y=-2$.

To visualize the flow fields produced by the TS wave shown in figure 5, we consider that when $\beta = 0$, the real velocity field produced by the TS wave may be written as,

$$\Re\left(\widehat{\mathbf{v}}\right) = \left[\widetilde{\mathbf{v}}_r(y)\cos(\alpha_r x) - \widetilde{\mathbf{v}}_i(y)\sin(\alpha_r x)\right]\mathrm{e}^{-\alpha_i x}. \tag{38}$$

Figure 6 shows the velocity vectors (panel a) and streamlines (panel b) produced by the TS wave

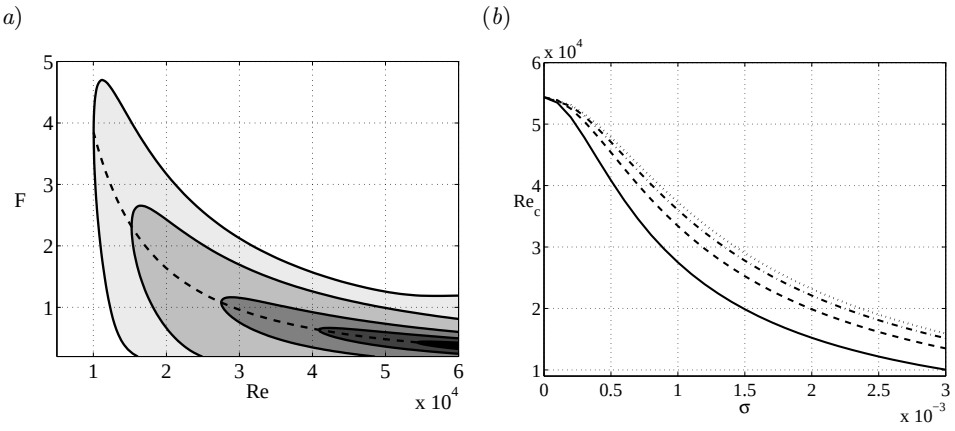

Fig. 7 (a) The neutral curves in the (Re, F) plane using the parameters $L_p = 2$, $\beta = 0$, and $\sigma = 0$, 0.0005, 0.001, 0.002, and 0.003. The unstable region for $\sigma = 0$ is shaded black. The unstable regions for $\sigma = 0.0005$ (darkest shade of grey), 0.001, 0.002 and 0.003 (lightest shade of grey) are shaded progressively lighter shades of grey. (b) The critical Reynolds number, Re_c, vs. σ using $L_p = 2$ (solid line), $L_p = 4$ (dashed line), $L_p = 6$ (dash-dotted line), $L_p = 8$ (dotted line).

in figure 5 when $\sigma = 0.003$. To aid the visualization, the exponential spatial growth of the wave, $\exp(-\alpha_i x)$, is ignored. Furthermore, because the perturbation magnitude in the boundary layer region ($y \geq 0$) is much larger than that in the porous layer and suction region ($y < 0$), the arrows representing the velocity vectors have been scaled up for $y < 0$, in comparison to the scaling used for $y > 0$. From figure 6, we observe that the TS wave is characterized by counter-rotating vortices in the boundary layer region, as well as vortical-type structures in the underlying porous layer and suction regions. The vortical structures in the porous layer and suction region are offset from those in boundary layer region, such that they appear roughly 90° out of phase. The streamlines in panel (b) suggest that the flow through the porous layer is primarily in the y-direction, except within the thin Brinkman layers.

Figure 7(a) illustrates the effects of a porous layer of thickness $L_p = 2$ on the neutral curve and unstable region in the (Re, F) plane of disturbances with spanwise wavenumber $\beta = 0$. The neutral curve for $\sigma = 0$ is illustrated in the lower right corner, with the unstable region shaded black. We found the critical point for $\sigma = 0$ at $(Re_c, F_c) = (54379.3, 0.4285)$, compared to $(Re_c, F_c) = (54370.0, 0.429)$ published by Hocking [23] and $(Re_c, F_c) = (54382.0, 0.429)$ published

by Fransson and Alfredsson [29]. Note that published values of the critical point for boundary layers in unbounded domains do not tend to agree as closely as those for Poiseuille or Couette flows due to the different methods used to satisfy the far-stream boundary conditions numerically. As σ increases from $\sigma_{min} = 0.0001$ to $\sigma_{max} = 0.003$, the critical point follows the dashed line in Fig. 7(a) from $(Re_c, F_c) = (53497.7, 0.4387)$ to $(Re_c, F_c) = (10035.4, 3.8436)$. The critical Reynolds number at σ_{max} is 18.45 % the critical Reynolds number for $\sigma = 0$. The neutral curves for $\sigma = 0.0005$, 0.001, 0.002 and 0.003 are illustrated with the unstable regions shaded progressively lighter shades of grey as σ increases. In addition to the decrease in critical Reynolds number with permeability, the size of the unstable regions grows substantially and, consequently, the band of unstable frequencies, F, for a given Reynolds number, increases drastically.

B. Effects of the Porous Layer Thickness, L_p

To characterize how the porous layer thickness, L_p, affects the linear stability of the ASBL, we repeat the calculation of the critical Reynolds number, Re_c, using the parameters $0.0001 \leq \sigma \leq 0.003$, $\beta = 0$, $L_p = 4$, 6, and 8. Figure 7(b) illustrates the results for Re_c using $L_p = 2$ (solid line), $L_p = 4$ (dashed line), $L_p = 6$ (dash-dotted line) and $L_p = 8$ (dotted line). We observe that the linear stability of the ASBL increase as L_p increases. At $\sigma_{max} = 0.003$, the critical Reynolds number was found to be $Re = 10035.4$ when $L_p = 2$, $Re = 13503.6$ when $L_p = 4$, $Re = 15160.2$ when $L_p = 6$, and $Re = 15926.3$ when $L_p = 8$. The increase in critical Reynolds number between $L_p = 6$ and $L_p = 8$ is much smaller than the increase between $L_p = 2$ and $L_p = 4$. This is explained by our observation that as L_p becomes large, $L_p \geq 8$, the porous layer behaves like a semi-infinite porous region, and the end effects at $y = -L_p$ become negligible.

Figures 8(a) and 8(b) illustrate $|\widetilde{v}|$ and $|\widetilde{p}|$, respectively, for $L_p = 2$ (solid line) and $L_p = 8$ (dashed line) using the fixed parameters $\sigma = 0.003$, $F = 0.803805$, $\beta = 0$, and $Re = 40000$. Note that the porous region for $L_p = 2$ has been shaded a darker shade of grey from that used for $L_p = 8$. We observe that $|\widetilde{v}|$ is significantly larger in the porous layer when $L_p = 2$ than when $L_p = 8$. Figure 8(b) demonstrates that this is due to the fact that the driving perturbation pressure gradient $d|\widetilde{p}|/dy$, across the porous layer, decreases as L_p increases. Though not shown, for brevity, we observe that $|\widetilde{u}|$ is not significantly affected by changes in L_p. The results illustrated in Fig. 8 are consistent with

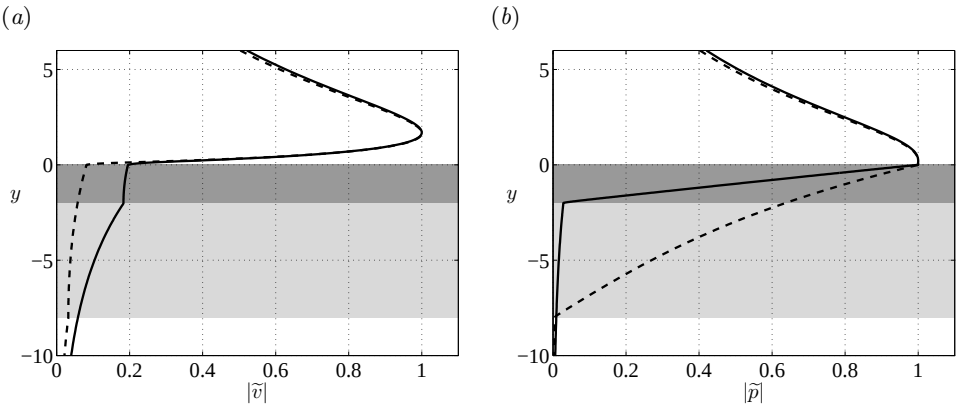

Fig. 8 Using the parameters $\sigma = 0.003$, $F = 2$, $\beta = 0$, and $Re = 40000$: (a) The eigenfunction $|\widetilde{v}|$ of the TS wave for $L_p = 2$ (solid line) and $L_p = 8$ (dashed line). The porous region for $L_p = 2$ is shaded the darkest shade of grey. (b) The eigenfunction $|\widetilde{p}|$ of the TS wave for $L_p = 2$ (solid line) and $L_p = 8$ (dashed line). The porous region for $L_p = 2$ is shaded the darkest shade of grey.

the hypothesis of Tilton and Cortelezzi [19] that the presence of a wall-normal disturbance velocity at an interface between a porous layer and a purely fluid region has a destabilizing effect, while the presence of a wall-tangential disturbance velocity at an interface is stabilizing. The increase in linear stability of the ASBL with increasing L_p may thus be explained by the observation that $|\widetilde{v}(0)|$ decreases while $|\widetilde{u}(0)|$ remains comparatively unchanged.

In a real laboratory experiment, the non-dimensional thickness L_p increases with the suction velocity, v_s. Consider, for example, a laboratory experiment in which σ is increased from $\sigma_{min} = 0.0001$ to $\sigma_{max} = 0.003$ by increasing the suction velocity from $v_{min} = 0.0001\nu/\sqrt{k}$ to $v_{max} = 0.003\nu/\sqrt{k}$. If $L_p = 2$ when $\sigma = 0.0001$, then $L_p = 60$ when $\sigma = 0.003$. Initial increases in σ near σ_{min} will produce critical Reynolds numbers near those illustrated as a solid line in Fig. 7(b) for $L_p = 2$. As the permeability increases further, the decrease in critical Reynolds number will be attenuated by the increase in L_p. Near σ_{max}, we would expect the critical Reynolds numbers to be slightly above those illustrated as a dashed line in Fig. 7(b) for $L_p = 8$.

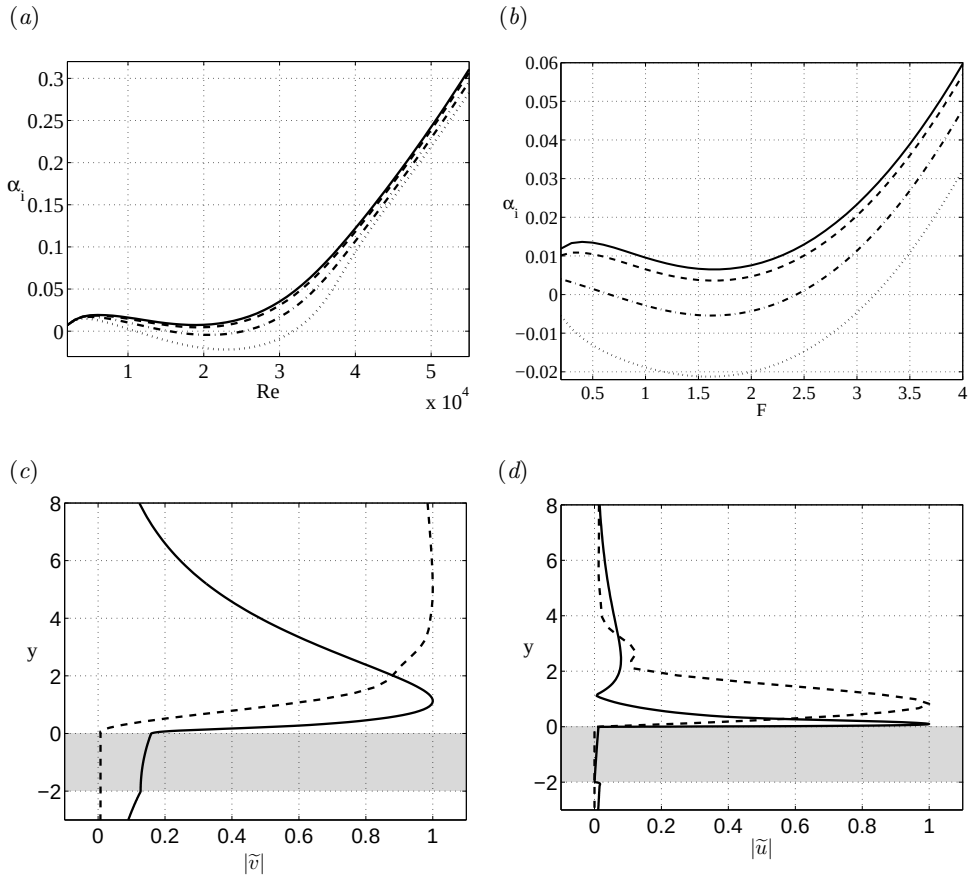

Fig. 9 (a) The damping factor, α_i, of the Tollmien-Schlichting wave vs. $\boldsymbol{Re}$ using the fixed parameters $L_p = 2$, $\beta = 0$, $F = 2.0$, $\sigma = 0$ (solid line), $\sigma = 0.001$ (dashed line), $\sigma = 0.002$ (dash-dotted line), $\sigma = 0.003$ (dotted line). The range of the Reynolds number is $2000 \leq \boldsymbol{Re} \leq 55000$. ($b$) The damping factor, α_i, of the Tollmien-Schlichting wave vs. F using the parameters $L_p = 2$, $\beta = 0$, $\boldsymbol{Re} = 20000$, $\sigma = 0$ (solid line), $\sigma = 0.001$ (dashed line), $\sigma = 0.002$ (dash-dotted line), $\sigma = 0.003$ (dotted line). The range of the frequency is $0.2 \leq F \leq 4.0$. (c) The magnitude $|\widetilde{v}|$ of the Tollmien-Schlichting eigenfunction for the parameters $L_p = 2$, $\sigma = 0.003$, $F = 2.0$, $\beta = 0$, $\boldsymbol{Re} = 2000$ (dashed line) and $\boldsymbol{Re} = 30000$ (solid line). (d) The magnitude $|\widetilde{u}|$ of the Tollmien-Schlichting eigenfunction for the parameters $L_p = 2$, $\sigma = 0.003$, $F = 2.0$, $\beta = 0$, $\boldsymbol{Re} = 2000$ (dashed line) and $\boldsymbol{Re} = 30000$ (solid line).

C. Effects of the Reynolds Number, Re, and Frequency, F

To characterize how the effects of permeability vary with Reynolds number, Re, and frequency, F, we compute the damping factor, α_i, of the TS wave using the parameters $0.2 \leq F \leq 4$, $2000 \leq Re \leq 55000$, $\beta = 0$, $L_p = 2$, and $\sigma = 0$, 0.001, 0.002, and 0.003. Figure 9(a) illustrates the behavior

of α_i as Re increases from 2000 to 55000 for fixed $F = 2.0$. Considering the neutral curves illustrated in Fig. 7(a), this corresponds to travelling along a horizontal line of constant $F = 2.0$ that intersects the neutral curves for $\sigma = 0.002$ and 0.003. In Fig. 9(a), therefore, the curves dip below $\alpha_i = 0$ when $\sigma = 0.002$ and 0.003. We observe that though permeability generally has a destabilizing effect, the effects become negligible below a Reynolds number around 2500. Figures 9(c) and 9(d) illustrate $|\widetilde{v}|$ and $|\widetilde{u}|$, respectively, of the TS wave at $Re = 2000$ (dashed line) and $Re = 30000$ (solid line) using the parameters $L_p = 2$, $\sigma = 0.003$, $F = 2.0$ and $\beta = 0$. When $Re = 30000$ (solid line), the magnitudes of the eigenfunctions are significant in the porous layer. For $Re = 2000$ (dashed line), however, the porous layer behaves like an impermeable wall, even though the permeability has been set to its maximum value.

Figure 9(b) illustrates the behavior of α_i as F increases from 0.2 to 4.0 for fixed $Re = 20000$. Considering the neutral curves illustrated in Fig. 7(a), this corresponds to travelling along a vertical line of constant $Re = 20000$ which intersects the neutral curves for $\sigma = 0.002$ and 0.003. In Fig. 9(b), therefore, the curves for α_i dip below $\alpha_i = 0$ when $\sigma = 0.002$ and 0.003. We again observe that permeability has a significant destabilizing effect.

D. Comparison With Experimental Results

Fransson and Alfredsson [29] have experimentally measured the characteristics of TS waves in an ASBL for the conditions $U_\infty = 5$ m s^{-1}, $\nu = 1.491$ x 10^{-5} m^2 s^{-1}, $d_1 = 0.00114$ m, $\beta = 0$, $F = 59$, and $Re = 382$. The porous layer was made of a sintered plastic material of thickness 0.0032 m (the non-dimensional thickness was $L_p = 2.807$) and permeability $k = 3.7$ x 10^{-12} m^2 (the non-dimensional permeability was $\sigma = 0.0017$). The porosity, ε, and interface coefficient, τ, are not known. Fransson and Alfredsson [29] found their experiments showed good agreement with the predictions of a spatial linear stability analysis that neglected wall permeability, i.e. they assumed $\sigma = 0$. The predicted TS eigenfunction, $\widetilde{u}(y)$, agreed well with the experimental measurements, and the predicted phase speed, $c = \omega/\alpha_r$, matched the experimental value, $c = 0.48U_\infty$. The only discrepancy involved the damping factor, α_i, for which the predicted value, $\alpha_i = 26.3$ m^{-1}, was 1.72 times higher than the experimentally measured value, $\alpha_i = 15.3$ m^{-1}. This was attributed to the combination of a slight adverse pressure gradient, a deviation in the laminar velocity profile due to

the presence of a spanwise slot, a low wave amplitude, and possible three-dimensional effects.

To compare the predictions of our model with those of Fransson and Alfredsson [29], we compute the spatial linear stability of the TS wave for the parameters $F = 59$, $\beta = 0$, $Re = 382$, $L_p = 2.807$, $\varepsilon = 0.95$, $\tau = 0.194$, $\sigma = 0$ and 0.0017. For these parameters, we find that permeability has a negligible effect. Our computations produce $\alpha = 0.046783 + \mathrm{i}0.030024$ when $\sigma = 0$, compared to $\alpha = 0.046832 + \mathrm{i}0.030012$ when $\sigma = 0.0017$, where α is non-dimensional. Both computations predict $c = 0.48U_\infty$ and $\alpha_i = 26.3$ m^{-1}. These computations use the properties of Foametal, $\varepsilon = 0.95$ and $\tau = 0.194$. Because Fransson and Alfredsson [29] used a sintered plastic material, we repeated our computations for the parameters $0.1 \leq \varepsilon \leq 0.9$ and $-1 \leq \tau \leq 1$, but found no appreciable difference in the results. From this comparison, we can conclude that our model correctly predicts that the effects of wall permeability become negligible for $Re \leq 2500$. This explains why the experimental results of Fransson and Alfredsson [29] show good agreement with theoretical results that neglect wall permeability. It is interesting to note that both our and Fransson and Alfredsson's [29] computations predict the same value for the damping factor α_i, a value that is 1.72 times higher than the experimentally measured value. This fact reinforces the reasons (reported above) provided by Fransson and Alfredsson [29] to explain this discrepancy in terms of experimental uncertainties.

VI. Conclusions

We performed a spatial linear stability analysis of the asymptotic suction boundary layer (ASBL) using a new model of wall suction. To this end, we modelled a porous wall as a layer of rigid, homogeneous, isotropic, porous material. The porous layer is bounded above by a semi-infinite fluid region in which a boundary layer is driven by a free-stream velocity, U_∞ at constant pressure P_∞. Wall suction is implemented by applying a suction pressure, P_s, lower than P_∞ in the boundary layer region, to a semi-infinite suction region below the porous layer. The fluid flows in the purely fluid regions were coupled to the flow in the porous region using the volume-averaged approach of Whitaker [40] and Ochoa-Tapia and Whitaker [41]. We restricted our study to small permeabilities for which inertial effects in the porous region could be neglected, and we fixed the porosity, $\varepsilon = 0.95$, and interface coefficient, $\tau = 0.194$, such that the porous material behaves like Foametal. The stability of the ASBL was computed for permeabilities ranging between $\sigma_{min} = 0.0001$ and

$\sigma_{max} = 0.003$, and for porous layers of non-dimensional thickness $2 \leq L_p \leq 8$.

We found that wall permeability destabilizes neither the Squire modes nor the continuous spectra, but significantly destabilizes the Tollmien-Schlichting (TS) wave. As the nondimensional permeability increases from σ_{min} to σ_{max}, for constant $\beta = 0$ and $L_p = 2$, the unstable region delimited by the neutral curve grows considerably, and the critical Reynolds number decreases from $Re_c = 53497.7$ at $\sigma_{min} = 0.0001$ to $Re_c = 10035.4$ at $\sigma_{max} = 0.003$. The critical Reynolds number at σ_{max} is only 18.45 % the corresponding value for $\sigma = 0$, which is $Re = 54379.3$. This decrease in stability is likely due to the effects of permeability on the wall-normal velocity of the TS wave. With increasing permeability, the magnitude of the wall-normal velocity of the TS wave increases within the porous layer. This wall-normal velocity is driven by the TS wave's pressure, whose magnitude $|\widetilde{p}|$ has a maximum at $y = 0$ and a nearly linear drop across the porous layer. In contrast, the streamwise velocity of the TS wave generally has a small magnitude within the porous layer.

We observed that the destabilizing effects of permeability decrease as the nondimensional thickness of the porous layer, L_p, increases. This occurs because an increase in L_p causes the wall-normal velocity of the TS wave to decrease within the porous layer. We also found that as L_p increases, the influence of L_p on the stability problem decreases because the porous layer behaves increasingly like a semi-infinite porous region.

To characterize how the effects of permeability vary with Reynolds number, Re, and frequency, F, we calculated the damping rate, α_i, of the TS wave for the parameters $0.2 \leq F \leq 4.0$, $2000 \leq Re \leq 55000$, $\beta = 0$, $L_p = 2$, and $\sigma = 0$, 0.001, 0.002, and 0.003. In this region of the parameter space, we found that the destabilizing effects of permeability increase with Reynolds number but become negligible below a Reynolds number of approximately $Re \approx 2000$. This explains why the previous experimental results of Fransson and Alfredsson [29] show excellent agreement with linear stability calculations that neglect the effects of wall permeability. Therefore, our model of wall suction captures both the stabilizing effects of wall suction and the destabilizing effects of wall permeability.

From our study, we can draw some important conclusions regarding the use of wall-suction for stabilizing boundary layers. Though our results confirm that wall-suction through a porous wall of

small permeability is a powerful means of stabilizing boundary layers and reducing wall turbulence, we find that wall-suction is far less powerful than as predicted by classical boundary layer stability theory. Classical theory, which neglects the effects of wall permeability, predicts that the best way to stabilize a boundary layer by suction is to apply suction through a porous wall having the largest possible permeability and smallest possible thickness. This choice maximizes the stabilization while minimizing the power required to produce the wall-suction. Our results, however, show that the mere presence of a porous wall substantially destabilizes the boundary layer flow over it, and that the level of destabilization increases as the permeability of the porous layer increases and as its thickness decreases. Therefore, from a stabilization point of view, it is desirable to choose a porous material of small permeability and sufficient thickness. From an operative point of view, however, the cost of applying suction increases as the permeability of the porous layer decreases and its thickness increases.

Consequently, we predict that there is an optimal operating condition, different from the maximum-permeability-minimum-thickness proposed by classical boundary layer theory, that obtains a maximum stabilization for minimum suction. A preliminary investigation of these optimal conditions may be found in reference [20], where it was determined that the optimization requires consideration of the upstream developing region of the ASBL. As this is beyond the scope of the current work, further consideration of these optimal conditions are left to future study. We want to emphasize, however, that maximum level of stabilization obtainable is much lower than the level predicted by the classical theory and the amount of suction needed much higher. In addition, while the current study focuses on a linear modal stability analysis, future studies of the effects of porous surfaces on by-pass transition, the ensuing non-linear regime, and fully developed turbulence, are all natural extensions of the current work.

Funding was provided by NSERC under a Postgraduate Scholarship and under Contract No. RGPIN217169.

References

[1] Tanner, M., "Reduction of Base Drag," *Progress in Aerospace Sciences*, Vol. 16, 1975, pp. 369-384.

[2] Savu, G., and Trifu, O., "Porous Airfoils in Transonic Flow," *AIAA Journal*, Vol. 22, 1984, pp. 989-991.

[3] Carpenter, P.W., and Porter, L.J., "Effects of Passive Porous Walls on Boundary-Layer Instability," *AIAA Journal*, Vol. 39, 2001, pp. 597-604.

[4] Hunter, C.A., Viken, S.A., Wood, R.M., and Bauer, S.X.S., "Advanced Aerodynamic Design of Passive Porosity Control Effectors," AIAA Paper 2001-0249, 2001.

[5] Tinetti, A. F., Kelly, J. J., Bauer, S. X. S., and Thomas, R. H., "On the Use of Surface Porosity to Reduce Unsteady Lift," AIAA Paper 2001-2921, 2001.

[6] Bauer, S. X. S., and Hemsch, M. J., "Alleviation of Side Force on Tangent-Ogive Forebodies Using Passive Porosity," *Journal of Aircraft*, Vol. 31, pp. 354-361,1993.

[7] Frink, N. T., Bonhaus, D. L., Vatsa, V. N., Bauer, S. X. S., and Tinetti, A. F., "Boundary Condition for Simulation of Flow Over Porous Surfaces," *Journal of Aircraft*, Vol. 40, 692-698, 2003.

[8] Ho, S., Nassef, H., Pornsinsirirak, N., Tai, Y-C., and Ho, C-M., "Unsteady Aerodynamics and Flow Control for Flapping Wing Flyers," *Progress in Aerospace Sciences*, Vol. 39, 2003, pp. 635-681.

[9] Lopera, J., Ng, T. T., and Patel, M. P., "Experimental Investigations of Reconfigurable Porosity for Aerodynamic Control," AIAA Paper 2004-2695, 2004.

[10] Kearney, J. M., and Glezer, A., "Aero-Effected Flight Control Using Distributed Active Bleed," AIAA Paper 2011-3099, 2011.

[11] Kearney, J. M., and Glezer, A., "Aerodynamic Control using Distributed Bleed," AIAA Paper 2012-3246, 2012.

[12] Joslin, R. D., "Aircraft Laminar Flow Control," *Annual Review of Fluid Mechanics*, Vol. 30, 1998, pp. 1-29.

[13] Joslin, R. D., "Overview of Laminar Flow Control," NASA TP-208705, 1998.

[14] Kim, J., "Control of Turbulent Boundary Layers," *Physics of Fluids*, Vol. 15, 2003, pp. 1093-1105.

[15] Beavers, G. S., and Joseph, D. D., "Boundary Conditions at a Naturally Permeable Wall," *Journal of Fluid Mechanics*, Vol. 30, 1967, pp. 197-207.

[16] Beavers, G. S., Sparrow, E. M., and Magnuson, R. A., "Experiments on Coupled Parallel Flows in a Channel and a Bounding Porous Medium," *Journal of Basic Engineering* (Trans. ASME), Vol. 92, 1970, pp. 843-848.

[17] Sparrow, E. M., Beavers, G. S., Chen, T. S., and Lloyd, J. R., "Breakdown of the Laminar Flow Regime in Permeable-Walled Ducts," *Journal of Applied Mechanics*, Vol. 40, 1973, pp. 337-342.

[18] Tilton, N., and Cortelezzi, L., "The Destabilizing Effects of Wall Permeability in Channel Flows: A Linear Stability Analysis," *Physics of Fluids*, Vol. 18, 2006, 051702.

[19] Tilton, N., and Cortelezzi, L., "Linear Stability Analysis of Pressure Driven Flows in Channels With Porous Walls," *Journal of Fluid Mechanics*, Vol. 604, 2008, pp. 411-445.

[20] Tilton, N., "The Effects of Wall Permeability on the Linear Stability of Channel Flows and the Asymptotic Suction Boundary Layer," Ph.D. Dissertation, Dept. Mechanical Engineering, McGill University, Montreal, QC, Canada, 2009.

[21] Schlichting H., *Boundary Layer Theory*, 7'$^{\text{th}}$ ed., McGraw-Hill, New York, 1979.

[22] Kay, J. M. "Boundary-Layer Flow Along a Flat Plate With Uniform Suction." Aeronautical Research Council Reports and Memoranda No. 2628, 1953.

[23] Hocking, L. M., "Non-Linear Instability of the Asymptotic Suction Velocity Profile," *Quarterly Journal of Mechanics and Applied Mathematics*, Vol. 28, 1975, pp. 341-353.

[24] Jordinson, R., "The Flat Plate Boundary Layer. Part 1. Numerical Integration of the Orr-Sommerfeld Equation,' *Journal of Fluid Mechanics*, Vol. 43, 1970, pp. 801-811.

[25] Saric, W. S., and Reed, H. L., "Effect of Suction and Week Mass Injection on Boundary-Layer Transition," *AIAA Journal*, Vol. 24, 1986, pp. 383-389.

[26] MacManus, D. G., and Eaton, J. A., "Flow Physics of Discrete Boundary Layer Suction - Measurements and Predictions," *Journal of Fluid Mechanics*, Vol. 417, 2000, pp. 47-75.

[27] Gregory, N., "Research on Suction Surfaces for Laminar Flow," *Boundary Layer and Flow Control*, edited by G.V. Lachmann, Pergamon Press, New York, 1961.

[28] Reynolds, G. A., and Saric, W. S., "Experiments on the Stability of the Flat-Plate Boundary Layer With Suction," *AIAA Journal*, Vol. 24, 1986, pp. 202-207.

[29] Fransson, J. F. M., and Alfredsson, P. H., "On the Disturbance Growth in an Asymptotic Suction Boundary Layer," *Journal of Fluid Mechanics*, Vol. 482, 2003, pp. 51-90.

[30] Braslow, A. L., Burrows, D. L., Tetervin, N., and Visconti, F., "Experimental and Theoretical Studies of Area Suction for the Control of the Laminar Boundary Layer on an NACA 64A010 Airfoil," NACA Report No. 1025, 1951.

[31] Reed, L. H., and Nayfeh, A. H., "Numerical-Perturbation Technique for Stability of Flat-Plate Boundary Layers With Suction," *AIAA Journal*, Vol. 24, 1986, pp. 208-214.

[32] Braslow, A. L., and Fischer, M. C., "Design Considerations for Application of Laminar Flow Control Systems to Transport Aircraft," AGARD Report No. 723, 1985, 4.1-4.27.

[33] Braslow, A., "A History of Suction-Type Laminar-Flow Control With Emphasis on Flight Research," NASA Monographs in Aerospace History No. 13, 1999.

[34] Arwatz, G., Fono, I., and Seifert, A., "Suction and Oscillatory Blowing Actuator Modeling and Valida-

tion," *AIAA Journal*, Vol. 46, 2008, pp. 1107-1117.

[35] Yoshioka, S., Fransson, J. H. M., and Alfredsson, P. H., "Free Stream Turbulence Induced Disturbances in Boundary Layers With Wall Suction," *Physics of Fluids*, Vol. 16, 2004, pp. 3530-3539.

[36] Levin, O., Davidsson, E. N., and Henningson, D. S., "Transition Thresholds in the Asymptotic Suction Boundary Layer," *Physics of Fluids*, Vol. 17, 2005, 114104.

[37] Byström, M. G., Levin, O., and Henningson, D. S., "Optimal Disturbances in Suction Boundary Layers," *European Journal of Mechanocs B-Fluids*, Vol. 26, 2006, pp. 330-343.

[38] Levin, O., and Henningson, D. S., "Turbulent Spots in the Asymptotic Suction Boundary Layer," *Journal of Fluid Mechanics,* Vol. 584, 2007, pp. 397-413.

[39] Davidsson, E. N., and Gustavsson, L. H., "Elementary Solutions for Streaky Structures in Boundary Layers With and Without Suction," *Fluid Dynamics Research*, Vol 40, 2007, pp. 212-231.

[40] Whitaker, S., "The Forchheimer Equation: A Theoretical Development," *Transport in Porous Media*, Vol. 25, 1996, pp. 27-61.

[41] Ochoa-Tapia, J. A., and Whitaker, S., "Momentum Transfer at the Boundary Between a Porous Medium and a Homogeneous Fluid-I. Theoretical Development," *International Journal of Heat Mass Transfer*, Vol. 38, 1995, pp. 2635-2646.

[42] Lage, J. L. "The fundamental theory of flow through permeable media from Darcy to turbulence," *Transport Phenomena in Porous Media*, edited by D. B. Ingham and I. Pop, Pergamon, Oxford, 1998

[43] Ochoa-Tapia, J. A., and Whitaker, S., "Momentum Transfer at the Boundary Between a Porous Medium and a Homogeneous Fluid-II. Comparison with Experiment," *International Journal of Heat Mass Transfer*, Vol. 38, 1995, pp. 2647-2655.

[44] Ochoa-Tapia, J. A., and Whitaker, S., "Momentum Jump Condition at a Boundary Between a Porous Medium and a Homogeneous Fluid: Inertial Effects," *Journal of Porous Media*, Vol. 1, 1998, pp. 201-217.

[45] Valdés-Parada, F.J., Goyeau, B., and Ochoa-Tapia, J. A., "Jump momentum boundary condition at a fluid-porous dividing surface: Derivation of the closure problem," *Chemical Engineering Science*, Vol. 62, 2007, pp. 4025-4039.

[46] Valdés-Parada, F.J., Aguilar-Madera, C.G., Ochoa-Tapia, J. A., and Goyeau, B., "Velocity and stress jump conditions between a porous medium and a fluid," *Advances in Water Resources*, Vol. 62, 2013, pp. 327-339.

[47] Breugem W. P., Boersma B. J. and Uittenbogaard, R. E., "The Laminar Boundary Layer over a Permeable Wall," *Transport in Porous Media*, Vol. 59, 2005, pp. 267-300.

[48] Gaponov, S. A., "Effect of the Properties of a Porous Coating on Boundary Layer Stability," NASA TM-75235, 1978.

[49] Lekoudis, S. G., "Stability of Boundary Layers Over Permeable Surfaces," AIAA Paper 78-0203, 1978.

[50] Jordinson, R., "Spectrum of Eigenvalues of the Orr-Sommerfeld Equation for Blasius Flow," *Physics of Fluids*, Vol. 14, 1971, pp. 2535-2537.

[51] Mack L. M., "A Numerical Study of the Temporal Eigenvalue Spectrum of the Blasius Boundary Layer," *Journal of Fluid Mechanics*, Vol. 73, 1976, pp. 497-520.

[52] Schmid, P. J., and Henningson, D. S., *Stability and Transition in Shear Flows*, Vol. 142, Springer-Verlag, 2001

[53] Goharzadeh, A., Khalili, A., and Jørgensen, B. B., "Transition Layer Thickness at a Fluid-Porous Interface," *Physics of Fluids*, Vol. 17, 2005, 057102.